

Optimal Working Points of a Singlet-Triplet $S-T_-$ Qubit

Clement H. Wong, M. A. Eriksson, S. N. Coppersmith, and Mark Friesen
Department of Physics, University of Wisconsin-Madison, Madison, Wisconsin 53706, USA
(Dated: December 7, 2024)

We propose an optimal set of quantum gates for a singlet-triplet qubit in a double quantum dot with two electrons utilizing the $S-T_-$ subspace. Qubit rotations are driven by the applied magnetic field and an orthogonal field gradient provided by a micromagnet. We optimize the fidelity of this qubit as a function of magnetic fields, taking advantage of “sweet spots” where the rotation frequencies are independent of the energy level detuning, providing protection against charge noise. We simulate gate operations and qubit rotations in the presence of quasistatic noise from charge and nuclear spins as well as leakage to nonqubit states, and predict that in silicon quantum dots gate fidelities greater than 99% can be achieved for two nearly-orthogonal rotation axes.

Electron spins in semiconductor quantum dots are promising qubits because of the long coherence times found in such devices and their potential for scalability [1]. Single-electron spins have been manipulated by applied AC magnetic fields in both III-V and group-IV devices [2–4]. By incorporating micromagnets [5] near the quantum dot, AC electric fields can be used for coherent manipulation of single spins [6,7]. Magnetic field differences can also be generated by pumping of the nuclear spin bath [8,9], or effective fields can be created by electric-field motion in high spin-orbit materials [10].

By working with two electrons in a double quantum dot, qubits can be formed from the singlet S and triplet T_0 states [9,11–14]. A magnetic field difference between the quantum dots enables full control of the $S-T_0$ subspace by controlling the detuning energy ϵ between the dots, with the eigenstates varying from $\{\downarrow\uparrow, \uparrow\downarrow\}$ to $\{S, T_0\}$ in different working regimes. Recently, an alternative two-electron qubit has been studied, consisting of the singlet S and polarized triplet T_+ states for GaAs [15–21] or the S and T_- states for Si [14]. Coherent oscillations have been observed in experiment [18], and theory predicts that such oscillations can be high speed [19]. However, it remains unclear whether this qubit can achieve fidelities high enough to meet the threshold for quantum error correction.

In this letter, we determine optimal working points for pulsed-gating manipulation of the $S-T_-$ (or, equivalently, $S-T_+$) qubit. We demonstrate that at these points, and using realistic assumptions about experimental noise derived from recent experiments, control fidelities in excess of 99% can be realized in natural abundance Si. The calculated fidelities are high enough to achieve fault-tolerant operation using surface code error correction [22]. Interestingly, only one of the optimal operating points is at a charge-noise sweet spot. The other optimal point is detuned from the second charge-noise sweet spot, in order to avoid leakage driven by the magnetic field difference between the quantum dots. Using realistic parameters, we find gate speeds of 43 MHz for X -rotations and 124 MHz for Z -rotations.

We consider a DC pulsed-gated $S-T_-$ qubit in an applied magnetic field gradient, as illustrated in Fig. 1. A typical double dot geometry incorporating a micromag-

net is shown in Fig. 1(a). There are three contributions to the total field: the uniform external field \mathbf{B}^{ext} , whose magnitude and direction are assumed to be tunable, the field from a micromagnet \mathbf{B}^{m} [5,14], and the slowly varying Overhauser fields arising from the nuclear spins [24]. We define our quantization axes with respect to the constant fields and consider the effects of Overhauser fields later. The \hat{z} quantization axis is defined along the average field direction $\mathbf{B}_{\text{avg}}=(\mathbf{B}_L + \mathbf{B}_R)/2=B_z\hat{z}$, and the micromagnet field difference is defined as $\Delta\mathbf{B}=\mathbf{B}_L^{\text{m}} - \mathbf{B}_R^{\text{m}}$, where L and R refer to local fields in the left and right dots. The relevant energy levels of the two-electron double dot as a function of the detuning ϵ , including energy splittings due to $\Delta\mathbf{B}$, are sketched in Fig. 1(c). The logical $S-T_-$ qubit is defined as the subspace of the two lowest-energy states when $\Delta\mathbf{B}=0$. We represent the qubit on a Bloch sphere with $|S\rangle$ ($|T_- \rangle$) on the north (south) poles. Rotations about two nearly orthogonal axes are performed at the detuning where the $S-T_-$ energy levels cross, labeled ϵ_X , and at a large negative detuning, labeled $\epsilon_{Z'}$. Figure 1(b) shows the singlet-triplet energy splittings near the $S-T_-$ crossing, with transitions due to $\Delta\mathbf{B}$ indicated. $S-T_0$ oscillations, driven by ΔB_z , correspond to leakage outside the $S-T_-$ qubit subspace. We suppress this process by arranging \mathbf{B}^{ext} such that $\Delta\mathbf{B} \perp \mathbf{B}^{\text{avg}}$ [25]. Then, for convenience, we define the x -axis such that $\Delta\mathbf{B}=\Delta B_x\hat{x}$, which mainly drives $S-T_-$ oscillations. For our choice of axes, the action of ΔB_x corresponds to an X -rotation on the Bloch sphere, while B_z and the exchange interaction J combine to produce Z -rotations, as illustrated in Fig. 1(b).

To investigate the rotation fidelities of the $S-T_-$ qubit, we consider a five-dimensional (5D) Hamiltonian [15,26, 27]. In addition to the static fields \mathbf{B}^{ext} and \mathbf{B}^{m} , the Hamiltonian includes nuclear fields \mathbf{h}_L and \mathbf{h}_R , as well as the nuclear field difference $\Delta\mathbf{h}=\mathbf{h}_L - \mathbf{h}_R$, which mixes the spin states. The main control parameter for the Hamiltonian is the relative energy detuning ϵ between the $(0, 2)$ and $(1, 1)$ charge states, as indicated in Fig. 1(c). Here, $\epsilon=0$ corresponds to the charging transition. Two detuning sweet spots defined by $\partial E_{01}/\partial\epsilon=0$ are apparent from the energy level diagram, where E_{01} is the energy gap between $|0\rangle$ and $|1\rangle$. The first sweet spot occurs at the anticrossing $\epsilon=\epsilon_X$. Simulations described below suggest

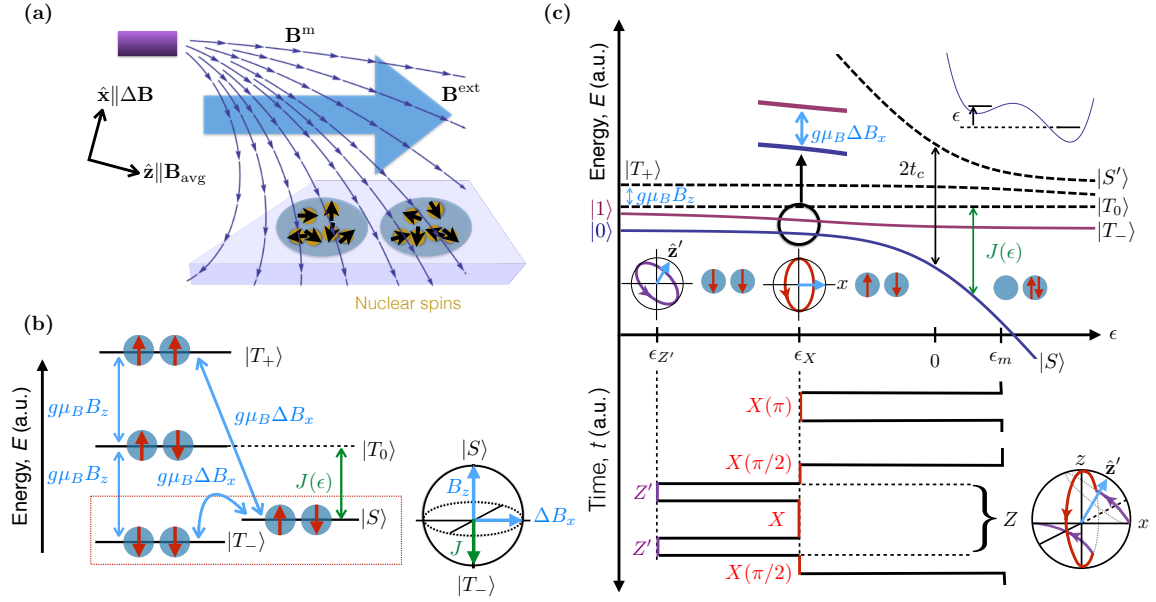


FIG. 1: (color online). (a) Illustration of a nonuniform magnetic field \mathbf{B}^m provided by a micromagnet (purple rectangle) fabricated above a double quantum dot, and a uniform external field \mathbf{B}^{ext} (blue arrow). Nonuniform Overhauser fields are also present, due to nuclear spins. (b) Singlet-triplet energy diagram, showing the dominant couplings between levels (arrows). A Bloch sphere representation of the S - T_- qubit indicates the rotation axes associated with the different coupling terms. (c) Top: singlet-triplet energy diagram as a function of detuning ϵ . X -rotations are performed at a detuning sweet spot (black circle at ϵ_X) where the qubit energy levels are parallel and the splitting is set by ΔB_x . Z' -rotations occur in the far-detuned regime ($\epsilon_{Z'}$), with a rotation axis \hat{z}' tilted slightly away from \hat{z} on the Bloch sphere. Bottom: illustration of typical pulse sequences for implementing X and Z -rotations. Measurement of the singlet probability is done at the detuning $\epsilon_m > 0$ in the $(0, 2)$ charge state. The Z protocol shows a Ramsey pulse sequence where the Z -rotation is implemented using a three-step sequence [23] to correct for the tilt of \hat{z}' , as illustrated on the Bloch sphere.

that this sweet spot is broadest and most effective at suppressing noise when the relation $\Delta B_x < B_z \ll t_c$ is satisfied, where t_c is the tunnel coupling between the dots. The second sweet spot occurs in the limit $\epsilon \rightarrow -\infty$; however our optimization shows that a higher fidelity can be achieved at a working point at finite detuning $\epsilon_{Z'}$, as described below.

Results reported in this letter use the full 5D Hamiltonian that includes the states S , T_- , T_0 , T_+ , and S' to properly account for leakage in the time evolution. However it is instructive to consider the 2D Hamiltonian spanning the S - T_- subspace, which can be obtained by a lowest-order canonical transformation [15,27]:

$$H^{(ST_-)} = \quad (1)$$

$$- \begin{pmatrix} J & \frac{\cos \eta}{2\sqrt{2}} g\mu_B (\Delta B_x + \Delta h_+) \\ \frac{\cos \eta}{2\sqrt{2}} g\mu_B (\Delta B_x + \Delta h_-) & g\mu_B (B_z + h_z) \end{pmatrix}.$$

(Higher order terms are discussed in [26].) Here, μ_B is the Bohr magneton, $g \simeq 2$ is the effective g -factor in silicon, and $h_{\pm} = h_x \pm ih_y$. We note that the basis state $|S\rangle$ in Eq. (1) is a superposition of the $(1, 1)$ and $(0, 2)$ singlet charge configurations, where the $(1, 1)$ amplitude is given by $\cos \eta = 1/\sqrt{1 + (J/t_c)^2}$. The exchange interaction J represents the energy splitting between S and

T_- states in the absence of a magnetic field [26]: $J = (\epsilon/2) + \sqrt{(\epsilon/2)^2 + t_c^2}$. We consider two cases in our simulations: (i) a constant tunnel coupling, with $t_c = 20 \mu\text{eV}$, and (ii) a detuning-dependent exchange [28], with a prominent exponential dependence arising through the tunnel coupling: $t_c = t_0 \exp(\epsilon/\epsilon_0)$, with $t_0 = 20 \mu\text{eV}$ and $\epsilon_0 = 1.1 \text{ meV}$ chosen to match experimental data for Si [13]. The simulation results shown in Fig. 2 correspond to case (i), while results for case (ii) are reported in [26]. Similar results are obtained in both cases, but depend on the specific parameters used. We also note that since J and η depend on ϵ , Hamiltonian (1) enables full electrical control of the logical qubit through this single control parameter.

Simulations are performed by numerically integrating the time-dependent Schrödinger equation $i\hbar(\partial/\partial t)|\Psi\rangle = H|\Psi\rangle$ [26], using the full 5D Hamiltonian. The main noise sources in a double dot are typically assumed to be charge fluctuations [28,30] and low-frequency nuclear field fluctuations [27,29], both of which cause inhomogeneous broadening in time-averaged measurements. We account for these effects by performing many time evolutions, with different values of ϵ and \mathbf{h} , as appropriate for modeling quasistatic variations from their average values ($\epsilon = \epsilon_X$ or $\epsilon_{Z'}$, and $\mathbf{h} = 0$, respectively). We then perform

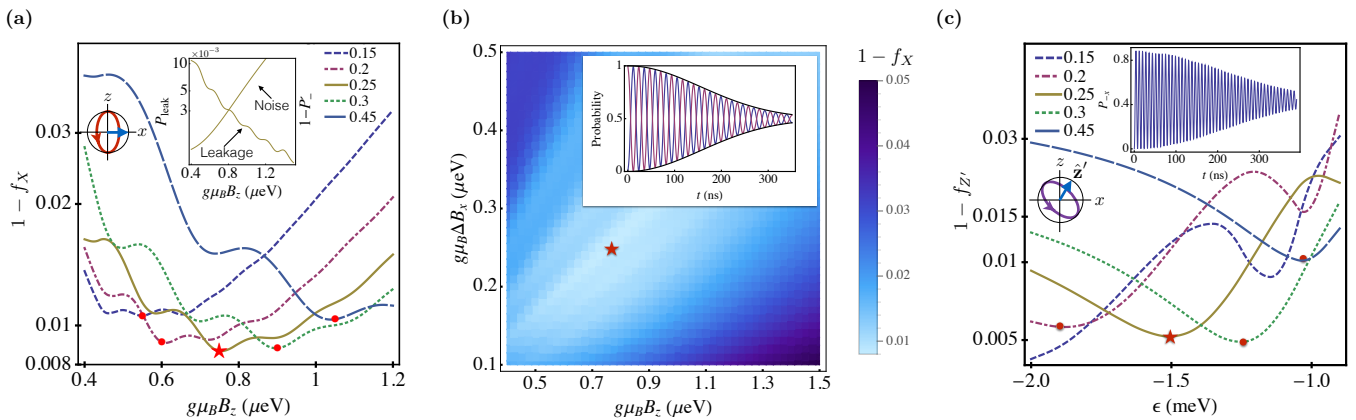


FIG. 2: (color online). (a) Semilog plot of $1 - f_X$, the infidelity of an $X(\pi)$ rotation, as a function of applied longitudinal field B_z , for several values of the field gradient ΔB_x (indicated in the legend in units of μeV). Inset: a similar plot showing the contributions to the infidelity due to leakage P_{leak} , and the combined effect of charge and nuclear noise $1 - P'_-$ [26], for the case $g\mu_B \Delta B_x = 0.25$ μeV . (b) A color density plot of $1 - f_X$ for an $X(\pi)$ rotation, as a function of B_z and ΔB_x . The red star indicates the optimal working point $g\mu_B(\Delta B_x, B_z) = (0.25, 0.75)$ μeV . Inset: Larmor oscillations (X -rotations), and the corresponding Gaussian decay envelope, obtained at the optimal point. (c) Infidelity of $Z'(\pi)$ rotations as a function of detuning, for nearly-optimal values of $g\mu_B \Delta B_x$ (indicated in the legend in units of μeV) and $g\mu_B B_z$ (indicated by the red dots and star in (a)). Inset: Z' -rotations performed at the starred point in (b), for $\epsilon_{Z'} = -1.5$ meV .

Gaussian averages over the final state probabilities, with variances $\sigma_\epsilon = 5$ μeV [13,14,31] and $\sigma_h = 3$ neV [13,14,24], as appropriate for natural Si.

We first investigate the fidelity of a pulsed $X(\pi)$ rotation, using the pulse sequence shown in the lower portion of Fig. 1(c). The qubit is initialized to state $|S(0, 2)\rangle$ at the detuning value $\epsilon = \epsilon_m$. The qubit is then pulsed via “rapid adiabatic passage” (RAP) [11] (fast compared to the S - T_- rotation frequency but slow compared to the tunneling frequency t_c) to the state $|S\rangle$ at the level anti-crossing ϵ_X , defined by $J(\epsilon_X) = g\mu_B B_z$. For the parameter values at which the gate fidelity is optimized, the RAP ramp from $(0, 2)$ to $(1, 1)$ can be performed so that its contribution to the infidelity due to leakage is negligible ($< 0.1\%$). We then evolve the system at $\epsilon = \epsilon_X$, perform averages over the quasistatic charge and nuclear noise distributions, and compute the average probabilities P_S , $P_{S'}$, P_\pm , and P_0 of being in the states $|S\rangle$, $|S'\rangle$, $|T_\pm\rangle$ and $|T_0\rangle$. Since $|T_- \rangle$ is the target final state, $f_X = P_-$ and $1 - f_X$ represents the fidelity and the infidelity of the $X(\pi)$ rotation, respectively, including contributions from charge noise, nuclear noise, and leakage.

Figure 2 shows the results of our simulations as a function of the magnetic fields B_z and ΔB_x . Although ΔB_x is fixed for a given micromagnet, our goal is to establish its optimal value, to aid in designing real physical devices. Figures 2(a) and (b) show that X -rotation fidelities of 99% should be attainable for the S - T_- qubit, far larger than in recent experiments [14,21] or theoretical proposals [32]. Long-lived Larmor oscillations are shown in the inset of Fig. 2(b). For case (i), we identify the optimal working point as $g\mu_B \Delta B_x = 0.25$ μeV ($\Delta B_x = 1.5$ mT) and $g\mu_B B_z = 0.75$ μeV ($B_z = 4.5$ mT). This point is marked by a star in Fig. 2(b), and corresponds to a gate

speed of 43 MHz . In Fig. 2(b), we see the speed can be increased by a factor of 2-3 from its optimal value, with little degradation of the fidelity, by simultaneously increasing ΔB_x and B_z . One can further increase the gate speed with high fidelity by increasing t_c , while keeping $\Delta B_x < B_z \ll t_c$. In practice, ΔB_x can be as large as 30 mT [5], or 3.5 μeV .

The small oscillations in Fig. 2 arise from leakage to T_+ caused by ΔB_x . The effect can be suppressed by imposing a large Zeeman splitting, $g\mu_B B_z$. Since the leakage process is coherent, the gate fidelity can also be enhanced by choosing a gate period that is commensurate with the leakage period. Alternatively, it is possible to utilize the leakage state T_+ to form a qutrit, but this would require more control parameters than in the present setup.

In Fig. 2(a), we see that the infidelity goes through a minimum as a function of B_z for a given ΔB_x . The origin of this behavior can be understood from the inset, where we plot the competing contributions to the infidelity from leakage, defined as $P_{\text{leak}} = P_+ + P_0 + P_{S'}$ (left axis), and from noise due to inhomogeneous broadening, denoted by $1 - P'_-$ (right axis), which cause dephasing and small random misorientations of the rotation axis away from \hat{x} . P'_- is computed with an approximate formula given in (S15) of [26]. It shows that at the optimal point the dephasing rate is dominated by nuclear noise with dephasing time $T_2^{*(X)} = \sqrt{2}\hbar/\sigma_h = 310$ ns , as consistent with the inset of Fig. 2(b). Therefore, decreasing nuclear noise will further improve the coherence time. P'_- also contains a B_z -dependent contribution of order $(\sigma_J/\Delta B_x)^2$ due to detuning noise, where $\sigma_J = \sigma_\epsilon \partial J / \partial \epsilon|_{\epsilon_X} \approx (g\mu_B B_z/t_c)^2 \sigma_\epsilon$ is the exchange noise variance.

We have also studied the fidelity of pulsed $Z(\pi)$ rotations. We note that the presence of ΔB_x causes a rota-

tion axis (\hat{z}') that is tilted away from \hat{z} in the x - z plane by angle $\theta = \tan^{-1}[\Delta B_x / \sqrt{2}(B_z - J(\epsilon_{Z'}))]$. If desired, a true Z -rotation can be implemented via a three-step pulse sequence, provided that $\theta < 45^\circ$ [23]. A conventional Ramsey sequence itself contains three pulses, $X(\pi/2)$ - $Z(\pi)$ - $X(\pi/2)$, suggesting the multi-pulse sequence shown in Fig. 1(c). Here, we simulate just the $Z'(\pi)$ portion of this sequence. Beginning with the initial state $|\hat{x}\rangle = (|S\rangle + |T_-\rangle) / \sqrt{2}$, on the equator of the S - T_- Bloch sphere, we suddenly pulse to $\epsilon_{Z'}$ and evolve the system for a π rotation period. We then compute the rotation fidelity $f_{Z'} = P_{-x} / P_{-x}^0$, where P_{-x} and P_{-x}^0 are the probabilities of reaching the final state $|\hat{x}\rangle$ with and without noise averaging, respectively.

The results of our simulations are shown in Fig. 2(c). Here, we have used several nearly optimal magnetic field values for ΔB_x and B_z obtained for $X(\pi)$ rotations. We find an optimal fidelity of about 99.5% at $\epsilon_{Z'} \simeq -1.5$ meV, corresponding to a gate frequency of 124 MHz and a tilt angle of $\theta = 19.5^\circ$. The inset in Fig. 2(c) shows long-lived Z' oscillations with $T_2^{*(Z')} \simeq 300$ ns at the optimal point. Similar to $X(\pi)$ rotations, the optimal value of $\epsilon_{Z'}$ is determined by competing contributions to the infidelity, $1 - f_{Z'}$. For $|\epsilon_{Z'}|$ smaller than the optimal value, detuning noise dominates the infidelity, while in the far-detuned regime, leakage dominates the infidelity. As a result, the optimal working point occurs at finite $\epsilon_{Z'}$, away from the second detuning sweet spot at $\epsilon \rightarrow -\infty$, where $J \rightarrow 0$.

In contrast to the typical situation for S - T_0 qubits, the S - T_- qubit has similar gate speeds and fidelities for both axes of rotation, which could be advantageous for performing dynamical pulses that remove the quasistatic noise. Furthermore, at the detuning ϵ_X , the dephasing time T_2^* of the optimal S - T_- oscillations is always longer than that of the exchange oscillations of the S - T_0 qubit, when ΔB_x is replaced by ΔB_z .

In conclusion, we propose a singlet-triplet qubit in the S - T_- subspace, for which all the qubit rotations

are governed by magnetic fields. By simulating a quasistatic noise model, we have shown that in the regime $\Delta B_x < B_z \ll t_c$, the qubit is well protected from detuning noise when we use the sweet spot at the S - T_- crossing, yielding fidelities exceeding 99% for rotations around two nearly orthogonal axes.

The fidelities predicted here depend on the input parameters in the simulations, and they can potentially be enhanced in several ways. First, we can reduce the nuclear noise through isotopic purification or nuclear polarization [8,9,33,34]. We estimate that the dominant fidelity-limiting mechanism would switch from nuclear to detuning noise by using 99.5% isotopically purified ^{28}Si , corresponding to $\sigma_h < 0.2$ neV, and a dephasing time of $T_2^{*(X)} = 3.3$ μs for X -rotations [26]. Charge noise can be reduced by using special gate geometries [30]. Finally, all dephasing mechanisms considered here can be suppressed by enhancing the tunnel coupling, while simultaneously increasing the magnetic fields [26].

While the analysis here has focused on DC pulsed gates, AC resonant gates have some advantages [35]. In particular, they allow all qubit operations to be performed at the sweet spot ϵ_X , similar to recent experiments at a charge qubit sweet spot [36] that show significant improvements over DC gating. Finally, we note that in materials with large hyperfine or spin-orbit interactions (e.g., GaAs or InGaAs), the role of ΔB_x could be replaced by polarized nuclear spins or a large spin-orbit coupling [37].

This work was supported in part by NSF (PHY-1104660), NSF (DMR-1206915), ARO (W911NF-12-0607), and by the Intelligence Community Postdoctoral Research Fellowship Program. The views and conclusions contained in this document are those of the authors and should not be interpreted as necessarily representing the official policies or endorsements, either expressed or implied, of the U.S. Government.

¹ F. A. Zwanenburg, A. S. Dzurak, A. Morello, M. Y. Simmons, L. C. L. Hollenberg, G. Klimeck, S. Rogge, S. N. Coppersmith, and M. A. Eriksson, *Rev. Mod. Phys.* **85**, 961 (2013).
² F. H. L. Koppens, C. Buizert, K. J. Tielrooij, I. T. Vink, K. C. Nowack, T. Meunier, L. P. Kouwenhoven, and L. M. K. Vandersypen, *Nature* **442**, 766 (2006).
³ J. J. Pla, K. Y. Tan, J. P. Dehollain, W. H. Lim, J. J. L. Morton, D. N. Jamieson, A. S. Dzurak, and A. Morello, *Nature* **489**, 541 (2012).
⁴ M. Veldhorst, J. Hwang, C. Yang, A. Leenstra, B. de Ronde, J. Dehollain, J. Muhonen, F. Hudson, K. Itoh, A. Morello, and A. Dzurak, arXiv:1407.1950.
⁵ M. Pioro-Ladrière, T. Obata, Y. Tokura, Y.-S. Shin, T. Kubo, K. Yoshida, T. Taniyama, and S. Tarucha, *Nat. Phys.* **4**, 776 (2008).
⁶ K. C. Nowack, F. H. L. Koppens, Y. V. Nazarov, and L. M. K. Vandersypen, *Science* **318**, 1430 (2007).

⁷ E. Kawakami, P. Scarlino, D. R. Ward, F. R. Braakman, D. E. Savage, M. G. Lagally, M. Friesen, S. N. Coppersmith, M. A. Eriksson, and L. M. K. Vandersypen, *Nature Nano.* **9**, 666 (2014).
⁸ D. J. Reilly, J. M. Taylor, J. R. Petta, C. M. Marcus, M. P. Hanson, and A. C. Gossard, *Science* **321**, 817 (2008).
⁹ S. Foletti, H. Bluhm, D. Mahalu, V. Umansky, and A. Yacoby, *Nature Physics* **5**, 903 (2009).
¹⁰ K. D. Petersson, L. W. McFaul, M. D. Schroer, M. Jung, J. M. Taylor, A. A. Houck, and J. R. Petta, *Nature* **490**, 380 (2012).
¹¹ J. R. Petta, A. C. Johnson, J. M. Taylor, E. A. Laird, A. Yacoby, M. D. Lukin, C. M. Marcus, M. P. Hanson, and A. C. Gossard, *Science* **309**, 2180 (2005).
¹² H. Bluhm, S. Foletti, I. Neder, M. Rudner, D. Mahalu, V. Umansky, and A. Yacoby, *Nature Physics* **7**, 109 (2011).
¹³ B. M. Maune, M. G. Borselli, B. Huang, T. D. Ladd,

- P. W. Deelman, K. S. Holabird, A. A. Kiselev, I. Alvarado-Rodriguez, R. S. Ross, A. E. Schmitz, M. Sokolich, C. A. Watson, M. F. Gyure, and A. T. Hunter, *Nature* **481**, 344 (2012).
- ¹⁴ X. Wu, D. R. Ward, J. R. Prance, D. Kim, J. K. Gamble, R. T. Mohr, Z. Shi, D. E. Savage, M. G. Lagally, M. Friesen, S. N. Coppersmith, and M. A. Eriksson, *Proc. Nat. Acad. Sci.* **111**, 11938 (2014).
- ¹⁵ W. A. Coish and D. Loss, *Phys. Rev. B* **72**, 125337 (2005).
- ¹⁶ W. A. Coish and D. Loss, *Phys. Rev. B* **75**, 161302 (2007).
- ¹⁷ H. Ribeiro and G. Burkard, *Phys. Rev. Lett.* **102**, 216802 (2009).
- ¹⁸ J. R. Petta, H. Lu, and A. C. Gossard, *Science* **327**, 669 (2010).
- ¹⁹ H. Ribeiro, J. R. Petta, and G. Burkard, *Phys. Rev. B* **82**, 115445 (2010).
- ²⁰ L. Gaudreau, G. Granger, A. Kam, G. C. Aers, S. A. Studenikin, P. Zawadzki, M. Pioro-Ladrière, Z. R. Wasilewski, and A. S. Sachrajda, *Nature Physics* **8**, 54 (2012).
- ²¹ H. Ribeiro, G. Burkard, J. R. Petta, H. Lu, and A. C. Gossard, *Phys. Rev. Lett.* **110**, 086804 (2013).
- ²² A. G. Fowler, M. Mariani, J. M. Martinis, and A. N. Cleland, *Phys. Rev. A* **86**, 032324 (2012).
- ²³ R. Hanson and G. Burkard, *Phys. Rev. Lett.* **98**, 050502 (2007).
- ²⁴ L. V. C. Assali, H. M. Petrilli, R. B. Capaz, B. Koiller, X. Hu, and S. Das Sarma, *Phys. Rev. B* **83**, 165301 (2011).
- ²⁵ Although \mathbf{B}^{avg} is not in the plane of the quantum well, it will not induce unwanted magnetic quantization effects if the field is small. The field gradient can also be arranged to be in the plane of the dot to eliminate this problem.
- ²⁶ See Supplemental Materials at [\(link goes here\)](#).
- ²⁷ J. M. Taylor, J. R. Petta, A. C. Johnson, A. Yacoby, C. M. Marcus, and M. D. Lukin, *Phys. Rev. B* **76**, 035315 (2007).
- ²⁸ O. E. Dial, M. D. Shulman, S. P. Harvey, H. Bluhm, V. Umansky, and A. Yacoby, *Phys. Rev. Lett.* **110** (2013).
- ²⁹ I. A. Merkulov, A. L. Efros, and M. Rosen, *Phys. Rev. B* **65**, 205309 (2002).
- ³⁰ C. Buizert, F. H. L. Koppens, M. Pioro-Ladrière, H.-P. Tranitz, I. T. Vink, S. Tarucha, W. Wegscheider, and L. M. K. Vandersypen, *Phys. Rev. Lett.* **101**, 226603 (2008).
- ³¹ Z. Shi, C. B. Simmons, D. R. Ward, J. R. Prance, R. T. Mohr, T. S. Koh, J. K. Gamble, X. Wu, D. E. Savage, M. G. Lagally, M. Friesen, S. N. Coppersmith, and M. A. Eriksson, *Phys. Rev. B* **88**, 075416 (2013).
- ³² S. Chesi, Y.-D. Wang, J. Yoneda, T. Otsuka, S. Tarucha, and D. Loss, [arXiv:1405.7618](#).
- ³³ A. Brataas and E. I. Rashba, *Phys. Rev. B* **84**, 045301 (2011).
- ³⁴ J. R. Petta, J. M. Taylor, A. C. Johnson, A. Yacoby, M. D. Lukin, C. M. Marcus, M. P. Hanson, and A. C. Gossard, *Phys. Rev. Lett.* **100**, 067601 (2008).
- ³⁵ M. D. Shulman, S. P. Harvey, J. M. Nichol, S. D. Bartlett, A. C. Doherty, V. Umansky, and A. Yacoby, [arXiv:1405.0485](#).
- ³⁶ D. Kim, D. R. Ward, C. B. Simmons, J. King Gamble, R. Blume-Kohout, E. Nielsen, D. E. Savage, M. G. Lagally, M. Friesen, S. N. Coppersmith, and M. A. Eriksson, [arXiv:1407.7607](#).
- ³⁷ M. S. Rudner, I. Neder, L. S. Levitov, and B. I. Halperin, *Phys. Rev. B* **82**, 041311 (2010).

Supplementary material for “Optimal Working Points of a Singlet-Triplet S - T_- Qubit”

In these supplemental materials, we provide details about the calculations and simulations described in the main text. In Sec. A, we summarize the basis and corresponding Hamiltonian that we use to simulate the qubit dynamics. In Sec. B, we review the leading corrections to the effective qubit Hamiltonian, derived in [1]. In Sec. C, we present our numerical method for averaging over quasistatic noise. In Sec. D, we analyze qubit dephasing. In Sec. D 1, we obtain an analytical expression for the pure dephasing time T_2^* . In Sec. D 2, we identify the detuning sweet spots, evaluate T_2^* at the optimal working points and compare its values for S - T_0 and S - T_- qubits. In Sec. D 3, we find the limiting dephasing rate in the absence of nuclear noise, and estimate the level of isotopic purification for which detuning noise becomes the dominant dephasing mechanism. In Sec. D 4, we present an analytic solution to noise-averaged X -rotations which captures effects due to fluctuations of the precession axis. In Sec. E, we present an exact analytic solution to the noise-averaged Z' -rotation in the far-detuned limit.

Appendix A: Double dot Hamiltonian

We model two electrons in a double quantum dot with a Hubbard Hamiltonian [1,2]

$$H = \frac{t_c}{\sqrt{2}}(\tilde{c}_L^\dagger \tilde{c}_R + \tilde{c}_R^\dagger \tilde{c}_L) + g\mu_B \sum_{i=L,R} (\mathbf{B}_i + \mathbf{h}_i) \cdot \tilde{c}_i^\dagger \frac{\boldsymbol{\sigma}}{2} \tilde{c}_i - \sum_{i=L,R} \mu_i (n_{i\uparrow} + n_{i\downarrow}) + U n_{i\uparrow} n_{i\downarrow}, \quad (\text{A1})$$

where \tilde{c}_i is the two-component spinor annihilation operator for electrons at dot i , (L, R) denotes (left, right), $\boldsymbol{\sigma}$ are the Pauli matrices, $n_{i\sigma}$ is the electron number operator, μ_i are electrochemical potentials, \uparrow and \downarrow denote spin up and down along the average magnetic field direction, t_c is

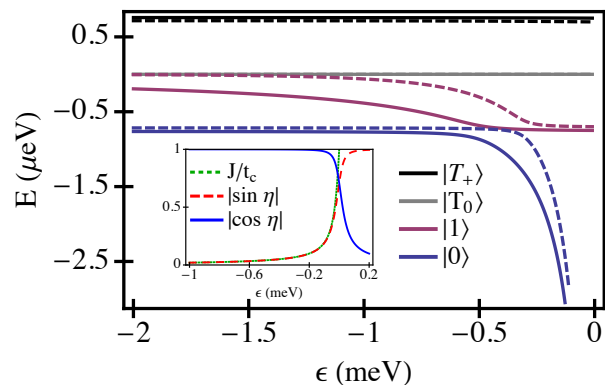


FIG. 3: Bold lines: The S - T_- qubit energy diagram including leakage states, as a function of detuning. The field parameters $g\mu_B(\Delta B_x, B_z) = (0.25, 0.75)$ μeV have been optimized for the constant tunnel coupling model with $t_c = 20$ μeV , as described in the main text. On the right-hand side of the anticrossing, we have $|0\rangle \simeq |S\rangle$ and $|1\rangle \simeq |T_- \rangle$. The high energy singlet $|S'\rangle$ is separated by a large energy splitting and lies outside the range of this plot. Dashed lines: The corresponding energy diagram for the field parameters $g\mu_B(\Delta B_x, B_z) = (0.3, 0.7)$ μeV , which are optimized for the detuning-dependent tunnel coupling model with $(t_0, \epsilon_0) = (20, 1100)$ μeV . Inset: The magnitudes of the charge mixing angles ($|\cos \eta|$, $|\sin \eta|$) [cf. Eq. (A2)] and exchange energy $J(\epsilon)$ [cf. Eq. (A3)].

the tunnel coupling, $g \simeq 2$ is the effective Landé electron g -factor in silicon, μ_B is the Bohr magneton, and U is the Coulomb interaction energy. An interdot Coulomb coupling can be included and absorbed into a redefinition of ϵ . The local applied magnetic fields and nuclear Overhauser fields are denoted by \mathbf{B}_i and \mathbf{h}_i , respectively. The detuning is defined by $\epsilon = \mu_L - \mu_R - U$, so that $\epsilon = 0$ corresponds to the $(1, 1) \rightarrow (0, 2)$ charge transition.

The Hamiltonian in the singlet subspace of $\{(1, 1), (0, 2)\}$ charge states is given by

$$H_S = t_c(|S(1, 1)\rangle\langle S(0, 2)| + \text{h.c.}) - \epsilon|S(0, 2)\rangle\langle S(0, 2)|.$$

The eigenstates are hybridized charge states given by

$$\begin{pmatrix} |S\rangle \\ |S'\rangle \end{pmatrix} = \begin{pmatrix} \cos \eta & \sin \eta \\ -\sin \eta & \cos \eta \end{pmatrix} \begin{pmatrix} |S(1, 1)\rangle \\ |S(0, 2)\rangle \end{pmatrix}, \quad (\text{A2})$$

with eigenvalues

$$\begin{pmatrix} E_S \\ E_{S'} \end{pmatrix} = t_c \begin{pmatrix} \tan \eta \\ -\cot \eta \end{pmatrix} = \frac{1}{2} \begin{pmatrix} -\epsilon - \sqrt{4t_c^2 + \epsilon^2} \\ -\epsilon + \sqrt{4t_c^2 + \epsilon^2} \end{pmatrix},$$

where we have parametrized the admixture of charge states by the mixing angle η , with $\cos \eta$ and $\sin \eta$ being the projections of $|S\rangle$ onto the $(1, 1)$ and $(0, 2)$ charge states, respectively. These projections can alternatively be expressed in terms of the singlet energies: $\cos \eta = 1/\sqrt{1 + (E_S/t_c)^2}$ and $\sin \eta = 1/\sqrt{1 + (E_{S'}/t_c)^2}$. We plot their magnitudes in the inset of Fig. 3. This hybridized basis is appropriate for the parameter regime where our qubit operates because the tunnel coupling is the largest energy scale in the problem [3]. The lower singlet state $|S\rangle$ approaches the unhybridized $|S(1, 1)\rangle$ state when $\epsilon \ll 0$, and it approaches $|S(0, 2)\rangle$ when $\epsilon \gg 0$, as shown in Fig. 1 of the main text. The excited singlet state $|S'\rangle$ has the opposite asymptotic behaviors. The exchange splitting is defined as the singlet-triplet splitting, given by

$$J(\epsilon) \equiv -E_g = -t_c \tan \eta = \frac{\epsilon}{2} + \sqrt{t_c^2 + \frac{\epsilon^2}{4}}. \quad (\text{A3})$$

In the inset of Fig. 3, we also plot the ratio J/t_c , showing that it closely matches $\sin \eta$. In the weak tunneling limit where $t_c \ll |\epsilon|$, Eq. (A3) gives $J(\epsilon) \approx t_c^2/|\epsilon|$. This power-law

behavior is consistent with experimental measurement in Ref. [4], over a range of detunings near the charge transition. The energy levels for constant t_c at the optimal magnetic fields given in the main text are plotted as a function of detuning in the main part of Fig. 3 (solid lines). The S' energy level is outside the range of the plot.

Recent experiments [4,5] suggest that the exchange energy may depend exponentially on the detuning in the far-detuned regime. To model the exchange energy consistent with these experiments, we also consider a tunnel coupling with exponential dependence on detuning, $t_c(\epsilon)=t_0 \exp(\epsilon/\epsilon_0)$. The energy diagram for $\epsilon_0=1.1$ meV at the corresponding optimal magnetic fields is shown with dashed lines in Fig. 3. This value of ϵ_0 is similar to that obtained by fitting data of the exchange energy $J(\epsilon)$ from Ref. [4] using the form given in Eq. (A3) with $t_c=t_c(\epsilon)$. This form of $J(\epsilon)$ drops more steeply near $\epsilon=0$ than the form with constant t_c , approaching zero at smaller detunings. Thus, the maximum value of $|\epsilon|$ for qubit operations, corresponding to the working point for Z' rotations (where $J \ll g\mu_B B_z$), occurs at smaller

values compared to the constant- t_c model. Table I (b), below, shows the resulting fidelities for the detuning-dependent tunnel coupling model, and their corresponding optimal magnetic fields. In general, the results for the detuning-dependent model are slightly worse the results of constant- t_c model reported in the main text, but can still yield fidelities exceeding 99%.

The Zeeman Hamiltonian in terms of the total spin $\mathbf{S}_L + \mathbf{S}_R$ and spin difference $\mathbf{S}_L - \mathbf{S}_R$ on the two dots is given by

$$H_Z = g\mu_B [\mathbf{B}_{\text{avg}} \cdot (\mathbf{S}_L + \mathbf{S}_R) + \frac{\Delta\mathbf{B}}{2} \cdot (\mathbf{S}_L - \mathbf{S}_R)], \quad (\text{A4})$$

where $\mathbf{S}_i = c_i^\dagger \boldsymbol{\sigma} c_i / 2$ ($i=L, R$) are the total spin operators for the left and right dots, $\mathbf{B}_{\text{avg}} = (\mathbf{B}_L + \mathbf{B}_R)/2$ and $\Delta\mathbf{B} = \mathbf{B}_L - \mathbf{B}_R$. As mentioned in the main text, we define the quantization axis ($\hat{\mathbf{z}}$) along the average applied magnetic field $\mathbf{B}_{\text{avg}} = B_z \hat{\mathbf{z}}$. For a general $\Delta\mathbf{B}$, the total Hamiltonian in the basis $\{T_+(1,1), T_0(1,1), T_-(1,1), S, S'\}$ is given by

$$H = g\mu_B \begin{pmatrix} B_z + h_z & h_+/2 & 0 & \cos \eta \frac{\Delta B_+ + \Delta h_+}{2\sqrt{2}} & -\sin \eta \frac{\Delta B_+ + \Delta h_+}{2\sqrt{2}} \\ h_-/2 & 0 & h_+/2 & \cos \eta \frac{\Delta B_z + \Delta h_z}{2} & -\sin \eta \frac{\Delta B_z + \Delta h_z}{2} \\ 0 & h_-/2 & -B_z - h_z & -\cos \eta \frac{\Delta B_- + \Delta h_-}{2\sqrt{2}} & \sin \eta \frac{\Delta B_- + \Delta h_-}{2\sqrt{2}} \\ \cos \eta \frac{\Delta B_- + \Delta h_-}{2\sqrt{2}} & \cos \eta \frac{\Delta B_z + \Delta h_z}{2} & -\cos \eta \frac{\Delta B_+ + \Delta h_+}{2\sqrt{2}} & \tan \eta (t_c/g\mu_B) & 0 \\ -\sin \eta \frac{\Delta B_- + \Delta h_-}{2\sqrt{2}} & -\sin \eta \frac{\Delta B_z + \Delta h_z}{2} & \sin \eta \frac{\Delta B_+ + \Delta h_+}{2\sqrt{2}} & 0 & -\cot \eta (t_c/g\mu_B) \end{pmatrix}, \quad (\text{A5})$$

where the singlet and triplet basis spin states are

$$|S\rangle = \frac{|\uparrow\downarrow\rangle - |\downarrow\uparrow\rangle}{\sqrt{2}}, \quad |T_0\rangle = \frac{|\uparrow\downarrow\rangle + |\downarrow\uparrow\rangle}{\sqrt{2}}, \\ |T_+\rangle = |\uparrow\uparrow\rangle, \quad |T_-\rangle = |\downarrow\downarrow\rangle,$$

and $\Delta B_\pm = \Delta B_x \pm i\Delta B_y$. $|S\rangle$ and $|S'\rangle$ have the same spin character but different charge character, as described below Eq. (A2). In Eq. (A5), we include only the tunnel coupling from $S(0,2)$ to $S(1,1)$ because the singlet-triplet tunneling is negligible, as spin-orbit coupling is very weak in silicon [6]. The energy diagram with optimal magnetic field values is plotted in Fig. 3.

From Eq. (A5), we see that the direct coupling between the S and the triplet states and between S' and the triplet states are proportional to the factors $\cos \eta$ and $\sin \eta$, respectively. The S -triplet coupling vanishes deep in the $(0,2)$ charge regime ($\epsilon \gg 0$), where $\cos \eta \rightarrow 0$ as shown in the inset in Fig. 3. In this regime, one can prepare the qubit in $|S\rangle$ without the mixing to triplets due to $\Delta\mathbf{B}$. On the other hand, the optimal qubit working points occur in the $(1,1)$ charge regime where $J/t_c \ll 1$ so that the approximation $(\cos \eta, \sin \eta) \approx (1, -J/t_c)$ is very accurate,

as shown in the inset of Fig. 3. In this regime, the leakage probability from the triplets to S' , proportional to $|\sin \eta|^2 \approx |J/t_c|^2 \approx 0$, are essentially zero. We confirm this in our numerical simulations, where the probability of occupying $|S'\rangle$ is found to be negligible. (See Sec. C.) Therefore, for the operating regime of interest ($J \ll t_c$), the relevant Hamiltonian is effectively reduced to the upper 4×4 block of Eq. (A5).

Appendix B: Effective S - T_- Hamiltonian

In this section, we derive an effective 2×2 Hamiltonian that includes corrections to Eq. (1) in the main text. These corrections are of order $(\Delta B_\pm)^2/B_z$, due to virtual transitions to T_0 and T_+ in second order perturbation theory [1]. As mentioned above, S' can be safely neglected in the $(1,1)$ regime, so we only need to consider the upper 4×4 block of Eq. (A5).

The effective Hamiltonian is defined as

$$H_{\text{eff}} = H^{(ST_-)} + \delta H^{(ST_-)},$$

where $H^{(ST_-)}$ is the lowest order term in the 2×2 Hamil-

tonian, as given in the main text, which is simply obtained by truncating terms outside the S - T_- manifold. The correction term is derived from nearly-degenerate perturbation theory [7] as

$$\delta H^{(ST_-)} = H_{PQ} \frac{1}{E - H_{QQ}} H_{QP}, \quad (\text{B1})$$

where $H_{PP} = PHP = H^{(ST_-)}$, $H_{QQ} = QHQ$, $H_{QP} = QHP$,

$H_{PQ} = PHQ$, $P = \sum_i |p_i\rangle\langle p_i|$ is the projection operator onto the S - T_- subspace with state labels p_i , and $Q = \sum_i |q_i\rangle\langle q_i|$ is the projection operator onto the T_0 - T_+ subspace with state labels q_i . To leading order in the correction, E corresponds to the average energy eigenvalue of $H^{(ST_-)}$. At the S - T_- crossing, we have $E = E_S = E_{T_-} = -B_z$. Thus, the energy denominator is given by

$$\frac{1}{E - H_{QQ}} = \text{diag} \left(\frac{1}{E_S - E_{T_+}}, \frac{1}{E_S - E_{T_0}} \right) = -\text{diag} \left(\frac{1}{2B_z}, \frac{1}{B_z} \right),$$

neglecting corrections of order h_{\pm}/B_z . From Eq. (A5), we have

$$H_{PQ} = \begin{pmatrix} \langle S|H|T_+ \rangle & \langle S|H|T_0 \rangle \\ \langle T_-|H|T_+ \rangle & \langle T_-|H|T_0 \rangle \end{pmatrix} = \begin{pmatrix} \cos \eta \frac{\Delta B_{\pm}}{2\sqrt{2}} & \cos \eta \frac{\Delta B_z}{2} \\ 0 & \frac{h_{\pm}}{2} \end{pmatrix},$$

and $H_{PQ} = H_{QP}^\dagger$. We then find that

$$\delta H_{ST} = -\frac{g\mu_B}{4B_z} \begin{pmatrix} \cos^2 \eta [(\Delta B_+ + \Delta h_+)(\Delta B_- + \Delta h_-)/4 + (\Delta B_z + \Delta h_z)^2] & \cos \eta h_- (\Delta B_z + \Delta h_z) \\ \cos \eta h_+ (\Delta B_z + \Delta h_z) & h_- h_+ \end{pmatrix}.$$

Thus, the leading order correction to H_{eff} is

$$\delta H_{ST}^{(0)} = -g\mu_B \cos^2 \eta \frac{\Delta B_+ \Delta B_- / 4 + \Delta B_z^2}{4B_z} \frac{1 + \tau_z}{2}. \quad (\text{B2})$$

This term slightly shifts the location of the S - T_- resonance, whose position is defined by $\text{Tr}[\tau_z H_{\text{eff}}(\epsilon_X)] = 0$, which now also depends on ΔB_{\pm} . However, in the optimal operating regime of the S - T_- qubit, we find that this correction is negligible.

Appendix C: Numerical Method for computing probabilities

The amplitudes c_n of occupying each state in the basis of Eq. (A5) are computed by numerically solving the Schrodinger equation

$$i\hbar \frac{dc_n}{dt} = \sum_{m=1}^5 H_{nm}(\xi_\alpha) c_m,$$

where c_n are the expansion coefficients of the wave function in the $\{T_+(1,1), T_0(1,1), T_-(1,1), S, S'\}$ basis, ξ_α are the quasistatic noise variables $\mathbf{h}_{L,R}$ and $\delta\epsilon$, and H_{nm} are the matrix elements given in Eq. (A5). Since we are interested in the regime $B_z > \Delta B_{\pm} \gg h_{\pm}$, the Rabi flopping terms due to the average fields h_{\pm} can be neglected. As described in the main text, we consider the case $\Delta B_z = 0$, and then assume $\Delta B_y = 0$

without loss of generality by orienting the x -axis along $\Delta \mathbf{B}$. We then compute $c_n(t)$ for a constant set of noise variables, and average the probabilities $|c_n|^2$ over Gaussian distributions $p(\xi_\alpha) = \exp(-\xi_\alpha^2/2\sigma_\alpha^2)/\sqrt{2\pi}\sigma_\alpha$ of the nuclear fields and detuning, with $\xi_\alpha \rightarrow (\epsilon, \Delta h_z, \Delta h_x, h_z)$ and the corresponding variances $\sigma_\alpha \rightarrow (\sigma_\epsilon, \sigma_{h_z}, \sigma_{\Delta h_z}, \sigma_{\Delta h_x}) = (5 \mu\text{eV}, \sigma_h, \sqrt{2}\sigma_h, \sqrt{2}\sigma_h)$, where $\sigma_h = 3 \text{ neV}$ and $\sigma_{\Delta h_x} = \sigma_{\Delta h_z} = \sqrt{2}\sigma_h$, as appropriate for uncorrelated noise between the left and right dots. We discretize the Gaussian average over the interval $\xi_\alpha \in [-3\sigma_\alpha, 3\sigma_\alpha]$ with a step size $\Delta\xi_\alpha = \sigma_\alpha$, so that the average probabilities (denoted by an overbar) are given by

$$P_n(t) = \overline{|c_n(t; \xi_\alpha)|^2} = \prod_{\alpha} \sum_{k_\alpha=-3}^3 p(\xi_\alpha) \Delta\xi_\alpha |c_n(t; \{\xi_\alpha = k_\alpha \sigma_\alpha\})|^2. \quad (\text{C1})$$

Table I(a) summarizes the parameter values used in the numerical simulations, yielding the results shown in the main text. Here, we assume the constant-tunnel coupling model with $t_c = 20 \mu\text{eV}$. For a smaller tunnel coupling, $t_c = 10 \mu\text{eV}$, we obtain an optimal fidelity of 98.4% when $g\mu_B(\Delta B_x, B_z) = (0.15, 0.3) \mu\text{eV}$. The optimal fidelities for the tunnel coupling model $t_c(\epsilon) = t_0 e^{\epsilon/\epsilon_0}$ are shown in Table I(b). In this case, we take $t_0 = 20 \mu\text{eV}$ and consider several values of ϵ_0 . When $\epsilon_0 \simeq 10 \text{ meV}$, we obtain fidelities of 99%, similar to the constant- t_c model. Further increasing ϵ_0 yields only marginal improvements in the

parameter	label	field (mT)	energy (μeV)
tunnel coupling	t_c	–	20
average field	B_z	6.47	0.75
difference field	$\Delta B_x/\sqrt{2}$	1.52	0.177
nuclear field variance	σ_h	0.026	0.003
detuning noise variance	σ_ϵ	–	5

(a)

ϵ_0 (μeV)	$g\mu_B\Delta B_x$ (μeV)	$g\mu_B B_z$ (μeV)	P_- (%)
1.1×10^3	0.3	0.7	98.47
10^4	0.3	0.9	99.06
10^6	0.3	0.9	99.14

(b)

TABLE I: (a) Relevant double dot parameters used in this analysis, including the tunnel coupling used in the constant- t_c model, the variances of the nuclear and detuning noise sources, and the resulting optimized fields. The different quantities are reported in units of magnetic fields (as appropriate) and energies. The nuclear noise variance is taken from Ref. [8], while the detuning noise variance is taken from Ref. [9]. (b) $X(\pi)$ gate fidelities (defined by the P_- probability described in the main text) at optimal magnetic fields, for the detuning-dependent tunnel coupling model $t_c(\epsilon)=t_0e^{\epsilon/\epsilon_0}$, with $t_0=20 \mu\text{eV}$ and three different values of ϵ_0 .

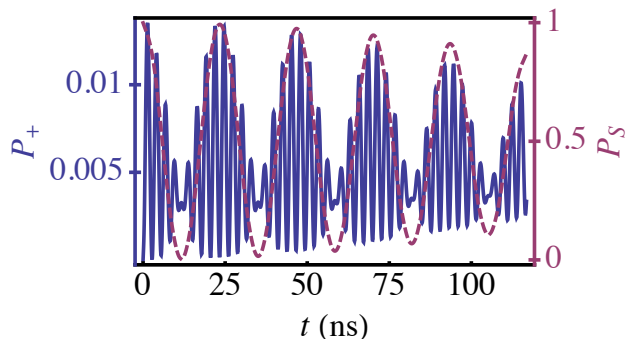


FIG. 4: Probability P_+ of leaking into the T_+ state as a function of time t during X -rotations, assuming $g\mu_B(\Delta B_x, B_z)=(0.25, 0.75) \mu\text{eV}$. The envelope of the oscillations closely follows the probability P_S of $|S\rangle$, shown as the maroon, dashed line (right-hand axis).

fidelity.

We end this section with a discussion of the leakage states T_+ , T_0 , and S' . The leakage probabilities for states T_0 and S' are of the order $P_0 \simeq 10^{-5}$ and $P_{S'} \simeq 10^{-10}$, respectively, which are negligible. The main leakage state is T_+ , and its probability during X -rotations is plotted in Fig. 4 for $g\mu_B(\Delta B_x, B_z)=(0.25, 0.75) \mu\text{eV}$. The results show an oscillation amplitude of about 1%. The leakage exhibits oscillations with two frequencies: the characteristic frequency of the leakage state, $2g\mu_B B_z/\hbar$, and the Larmor frequency for X -rotations, $g\mu_B \Delta B_x/\sqrt{2}\hbar$. The low frequency modulation is proportional to the singlet probability. We verify this by plotting the singlet probability P_S in Fig. 4 with dashed lines that clearly follow the envelope of the T_+ oscillations. The leakage probability is consistent with the transition probability from S to T_+ estimated from perturbation theory for short

times [10]:

$$P_+ \propto P_S \left(\frac{\Delta B_x}{B_z} \right)^2 \sin^2(g\mu_B B_z t/\hbar), \quad (\text{C2})$$

assuming an initial singlet probability of P_S . Note that the leakage envelope goes through a minimum at the end of the π pulse.

Appendix D: Qubit dephasing in the S - T_- subspace

In this section, we analyze the dephasing due to quasistatic variations of the fields and of the exchange coupling noise within the qubit subspace, focusing on the X -rotations. The qubit Hamiltonian, up to an overall shift in the energy, is given by $H^{(ST_-)} = (\mathbf{b} + \delta\mathbf{b}) \cdot \boldsymbol{\tau}/2$, where

$$\mathbf{b}(\epsilon) = -g\mu_B \left[\frac{\Delta B_x}{\sqrt{2}} \hat{\mathbf{x}} + \left(B_z - \frac{J(\epsilon)}{g\mu_B} \right) \hat{\mathbf{z}} \right] \quad (\text{D1})$$

is the effective field in the $\{S, T_-\}$ qubit subspace, and

$$\delta\mathbf{b} = -g\mu_B \left[\left(h_z - \frac{\delta J}{g\mu_B} \right) \hat{\mathbf{z}} + \frac{\Delta h_x}{\sqrt{2}} \hat{\mathbf{x}} + \frac{\Delta h_y}{\sqrt{2}} \hat{\mathbf{y}} \right] \quad (\text{D2})$$

is the field due to the noise terms. Here, we keep only the leading term in the effective Hamiltonian, and take $\cos \eta = 1$, as is appropriate near the working points of this qubit. In Eq. (D2), $\delta J = J(\epsilon + \delta\epsilon) - J(\epsilon)$ is the fluctuation in J arising from fluctuations of the detuning, $\delta\epsilon$. We denote by $\hat{\boldsymbol{\tau}}$ the Pauli matrices that span the S - T_- subspace. (For example, $\tau_z = |S\rangle\langle S| - |T_-\rangle\langle T_-|$.)

1. Pure dephasing rates

Here, we calculate the dephasing rate in the S - T_- subspace. The energy splitting between the energy eigenstates $|0\rangle$ and $|1\rangle$ is given by $E_{01} = |\mathbf{b}|$, and the fluctuation, up to quadratic order in the noise terms, is given by

$$\delta E_{01} \approx \delta b_{\parallel} + \frac{|\delta\mathbf{b}_{\perp}|^2}{2E_{01}}, \quad (\text{D3})$$

where $\delta b_{\parallel} = \delta \mathbf{b} \cdot \hat{\mathbf{b}}$ and $\delta \mathbf{b}_{\perp} = \delta \mathbf{b} - \delta b_{\parallel} \hat{\mathbf{b}}$ are the components of the noise field longitudinal and transverse to $\hat{\mathbf{b}} = \mathbf{b}/|\mathbf{b}|$, respectively. Note that the expansion in Eq. (D3) is only valid when $\delta E_{01}/E_{01} \ll 1$.

The pure dephasing time scales are computed by averaging the relative dynamical phase factor between $|0\rangle$ and $|1\rangle$ with respect to the noise terms:

$$\overline{e^{i(\delta E_{01}t)/\hbar}} = \overline{e^{i\delta b_{\parallel}t/\hbar} e^{i\delta \mathbf{b}_{\perp}^2/2E_{01}}} \quad (\text{D4})$$

$$= e^{-(t/T_2^*(\epsilon))^2} W_{\perp}(t)$$

$$\overline{e^{i\delta b_{\parallel}t/\hbar}} \equiv e^{-(t/T_2^*(\epsilon))^2}, \quad (\text{D5})$$

$$\overline{e^{i\delta \mathbf{b}_{\perp}^2/2E_{01}}} \equiv W_{\perp}(t), \quad (\text{D6})$$

where the overbar denotes a noise average. For Gaussian distributions of δb_i with variances σ_i , the average of a generic function $g(\delta \mathbf{b})$ is given by

$$\overline{g(\delta \mathbf{b})} = \prod_i \int \frac{d(\delta b_i)}{\sqrt{2\pi\sigma_i}} g(\delta \mathbf{b}) e^{-\delta b_i^2/2\sigma_i^2},$$

where $\overline{\delta b_i} = 0$, $\overline{\delta b_i \delta b_j} = \delta_{ij} \sigma_i^2$, and $i = x, y, z$. Because the noise in orthogonal directions are uncorrelated, the longitudinal and transverse averages in Eq. (D4) can be separated. We first consider the leading, longitudinal contribution which gives rise to $T_2^*(\epsilon)$. The function $W_{\perp}(t)$ is a decay envelope due to the subleading, transverse contribution that is only important when the longitudinal nuclear noise is significantly reduced. (We analyze this situation in Sec. D3, below.) Evaluating the average in Eq. (D5), one finds that

$$\frac{\sqrt{2}\hbar}{T_2^*(\epsilon)} = \sqrt{\left(\sigma_J(\epsilon) \frac{\partial E_{01}}{\partial J}\right)^2 + \sigma_h^2 \left[\left(\frac{\partial E_{01}}{\partial \Delta B_x}\right)^2 + \left(\frac{\partial E_{01}}{\partial B_z}\right)^2 \right]}$$

$$= \sqrt{\frac{(\sigma_h^2 + \sigma_J(\epsilon)^2)(J(\epsilon)/g\mu_B - B_z)^2 + \sigma_h^2 \Delta B_x^2/2}{(J(\epsilon)/g\mu_B - B_z)^2 + \Delta B_x^2/2}}, \quad (\text{D7})$$

where $\sigma_J(\epsilon) = (\partial J/\partial \epsilon) \sigma_{\epsilon}$ is the detuning-dependent variance in the exchange noise.

Eq. (D7) relies on the expansion given in Eq. (D3), which is only valid when $\delta E_{01}/E_{01} \ll 1$. The latter condition is not obviously true, *a priori*, since $\sigma_{\epsilon} \gg \Delta B_x, B_z$, and it is in the greatest danger of being violated at the $S-T_{-}$ anticrossing ϵ_X , where $E_{01} = g\mu_B \Delta B_x/\sqrt{2}$. However, the condition is satisfied when $g\mu_B B_z \ll t_c$, yielding an $S-T_{-}$ anticrossing at $\epsilon_X \approx -t_c^2/g\mu_B B_z$, which lies deep in the (1,1) charge regime, where the variance of J is significantly reduced:

$$\sigma_J(\epsilon_X) = \sigma_{\epsilon} \left(\frac{\partial J}{\partial \epsilon} \right)_{\epsilon=\epsilon_X} \approx \sigma_{\epsilon} \left(\frac{g\mu_B B_z}{t_c} \right)^2. \quad (\text{D8})$$

For $g\mu_B B_z = 0.75 \mu\text{eV}$, $\sigma_J \sim 7 \text{ neV}$ is very small for natural Si—of order of the nuclear Zeeman energy—and it can

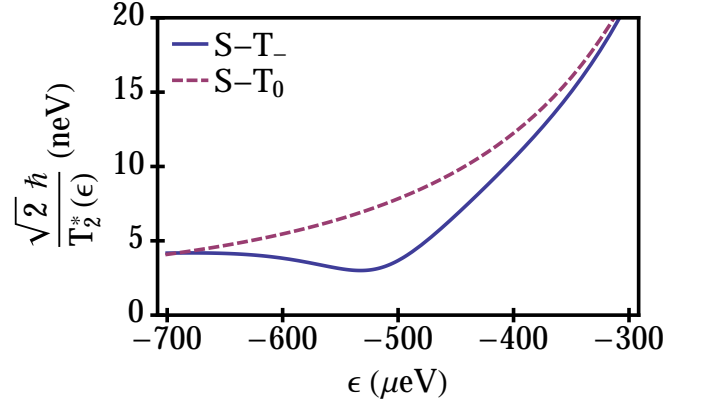


FIG. 5: A comparison of the dephasing rates for $S-T_0$ and $S-T_{-}$ qubits near the sweet spot ϵ_X , for optimal magnetic fields of the $S-T_{-}$ qubit, taking $\Delta B_z = \Delta B_x/\sqrt{2}$ for the $S-T_0$ qubit.

be further reduced by increasing t_c . Eq. (D7) thus holds for all detunings in the operating regime of this qubit. We also note that the charge noise associated with virtual occupation of the (0,2) state [11] is proportional to $\sin^2 \eta \approx (t_c/\epsilon_X)^2 \approx (g\mu_B B_z/t_c)^2 \ll 1$ and is therefore negligible.

2. Sweet spots and optimal working points

The detuning sweet spots described in the main text occur when $\partial E_{01}/\partial \epsilon = 0$. From Eq. (D1), we see that $\partial E_{01}/\partial \epsilon \propto (g\mu_B B_z - J)(\partial J/\partial \epsilon)$. One sweet spot therefore occurs at the anticrossing ϵ_X , defined by $J(\epsilon_X) = g\mu_B B_z$, while the second sweet spot occurs in the limit $\epsilon \rightarrow -\infty$, where $\partial J/\partial \epsilon \rightarrow 0$. At ϵ_X , we also have $\partial E_{01}/\partial B_z = 0$ and $\partial E_{01}/\partial (\Delta B_y) = 0$. Hence, ϵ_X is also a sweet spot for transverse fluctuations ($h_z, \Delta h_y$) of the nuclear field.

Naively, since detuning noise is the largest source of noise, one may expect the optimal working points of the $S-T_{-}$ qubit to occur at the detuning sweet spots where $T_2^*(\epsilon)$ is maximized. This is true at the sweet spot ϵ_X , yielding $T_2^{*(X)} = \sqrt{2}\hbar/\sigma_h = 310 \text{ ns}$. However, due to leakage out of the qubit subspace [See Eq. (C2)] which is not taken into account in this section, our numerical analysis shows that the optimal working point for Z' rotations occurs at a large but finite value of $-\epsilon$, at $\epsilon_{Z'} \approx -1.5 \text{ meV}$ for the constant- t_c model. At this point, Eq. (D7) gives the dephasing time $T_2^{*(Z')} \approx 300 \text{ ns}$, consistent with our numerical simulations.

The working point ϵ_X , for X -rotations of the $S-T_{-}$ qubit, is also near the working point for exchange-mediated rotations of the $S-T_0$ qubit. It is therefore interesting to compare the operations of these two qubits when $\epsilon = \epsilon_X$. Specifically, we compare the dephasing times $T_2^{*(X)}$. Equation (D7) describes this result for $S-T_{-}$ qubits. For $S-T_0$ qubits, the effective field acting on

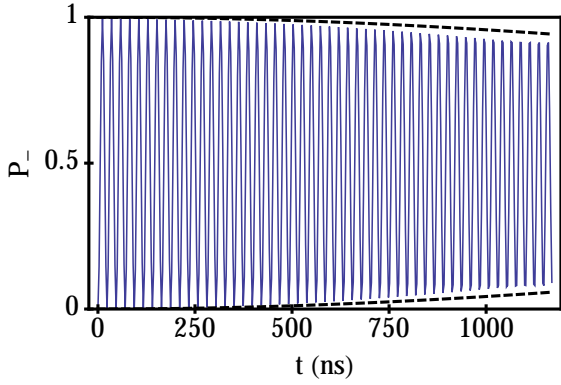


FIG. 6: The numerically computed probability P_- of occupying the T_- state as a function of time t during X -rotations in the absence of nuclear noise, for an initial singlet state S . The dephasing envelope (dashed lines) is given by Eq. (D11) with $\sigma_h = 0$.

the Bloch sphere is $\mathbf{b} = J\hat{\mathbf{z}} + g\mu_B\Delta B_z\hat{\mathbf{x}}$, which yields the following dephasing rate for S - T_0 qubits [5]:

$$\frac{\sqrt{2}\hbar}{T_2^{*(ST_0)}} = \sqrt{\frac{(\sigma_J(\epsilon)J)^2 + 2(\sigma_h g\mu_B\Delta B_z)^2}{J^2 + (g\mu_B\Delta B_z)^2}}.$$

We then plot the dephasing rates for S - T_0 and S - T_- qubits near the sweet spot ϵ_X in Fig. 5, for optimal magnetic fields of the S - T_- qubit. For the S - T_0 qubit we take $\Delta B_z = \Delta B_x / \sqrt{2}$, so that the two qubits have the same rotation frequencies. For these parameters, the sweet spot occurs at $\epsilon_X \approx 500$ μeV . In the figure, we see that the S - T_0 dephasing rate at ϵ_X is about twice as fast as that of the S - T_- qubit.

3. Dephasing in the absence of nuclear noise

As described in Sec. D 1, the dephasing rate for X -rotations is set by the longitudinal nuclear noise. However, if nuclear noise is removed by isotopic purification or dynamic polarization, the detuning noise remains as a dephasing mechanism. As mentioned in Sec. D 2, detuning noise ($\delta\epsilon$) at ϵ_X is transverse to the effective field of the Hamiltonian and appears at quadratic order in the energy fluctuations, as given in Eq. (D3), yielding the decay envelope $W_\perp(t)$ in Eq. (D6) which has a qualitatively different decay behavior than Eq. (D5). Here, we compare the contribution to the dephasing rate for X -rotations due to transverse and longitudinal noise, and determine the nuclear noise variance that marks the crossover between nuclear vs. detuning noise-dominated dephasing.

The decay envelope $W_\perp(t)$ at ϵ_X is derived by averaging over the quadratic fluctuations. The Gaussian inte-

gral can be solved exactly:

$$W_\perp(t) = \overline{e^{i\delta\mathbf{b}_\perp^2 t/2\hbar E_{01}}} = \prod_\alpha \frac{1}{\sqrt{1 - i\sigma_\alpha^2 t/\hbar b}} \approx e^{i\phi} e^{-\left(t/T_{2\perp}^{*(X)}\right)^2}, \quad (\sigma_\alpha^2 t/2\hbar b \ll 1), \quad (\text{D9})$$

where the product is over the two transverse noise sources σ_J and σ_h , ϕ is an irrelevant phase that plays no role when we compute state probabilities, $b = |\mathbf{b}(\epsilon_X)| = g\mu_B|\Delta B_x|/\sqrt{2}$ is the magnitude of the effective field of the Hamiltonian, and the transverse dephasing time is given by

$$T_{2\perp}^{*(X)} = \frac{2\hbar b}{\sigma_J^2 + \sigma_h^2}. \quad (\text{D10})$$

In the last line of Eq. (D9), we assume a short time limit, which is appropriate for the duration of a qubit gate ($\tau_x \sim 1/b$), since $\sigma^2\tau_x/\hbar b \sim \sigma^2/b^2 \ll 1$. If we denote the longitudinal dephasing time obtained in the previous section as $T_{2\parallel}^{*(X)} = \sqrt{2}\hbar/\sigma_h$, then the combined, short-time decay function at ϵ_X is given by

$$\exp\left(-\frac{t^2}{T_{2\perp}^{*(X)2}} - \frac{t^2}{T_{2\parallel}^{*(X)2}}\right). \quad (\text{D11})$$

Here, the shorter dephasing time naturally dominates the decay.

We now determine the crossover from nuclear to detuning noise-dominated decay, which can be implemented by isotopically purifying the sample with ^{28}Si . The ratio of the longitudinal and transverse dephasing times is given by

$$\frac{T_{2\parallel}^{*(X)}}{T_{2\perp}^{*(X)}} = \frac{\sigma_J^2}{\sqrt{2}b\sigma_h} \left[1 + \left(\frac{\sigma_h}{\sigma_J}\right)^2\right].$$

Solving for the crossover point which occurs when the ratio is equal to 1, we find $\sigma_h \approx \sigma_J^2/\sqrt{2}b = 0.2$ neV. This happens when the abundance of ^{29}Si is reduced from $\sim 5\%$ (natural abundance) to $\sim 0.5\%$. At this level of purification, the total dephasing time is given by $[(T_{2\parallel}^{*(X)})^{-2} + (T_{2\perp}^{*(X)})^{-2}]^{-1/2} = 3.3$ μs . In the limit of pure ^{28}Si , the maximum dephasing time is given by $T_{2\perp}^{*(X)} = 4.7$ μs , and is due entirely to the remaining detuning noise. We demonstrate this limit in Fig. 6, which shows the numerically computed P_- probability for X -rotations. The dephasing envelope is predicted by Eq. (D11) with $\sigma_h = 0$. Note that we have not re-optimized with respect to magnetic fields here, which could give further improvements in the coherence.

4. Infidelity due to fluctuations of precession axis

At the sweet spot ϵ_X , although detuning noise $\delta\epsilon$ does not contribute to the pure dephasing rate at leading order, it tilts the direction of the precession axis, causing

a small but finite infidelity. This effect is not captured by the decay envelope Eq.(D4), which includes only fluctuations in rotation frequency. More importantly, this type of infidelity coming from transverse noise is much larger than the infidelity coming from the higher order contribution to the pure dephasing rates studied in the previous section. In fact, this is the origin of the B_z dependence in the X -rotation infidelity shown in Fig. 2 (a) and (b) of the main text. As noted in the main text, the competition between this effect and leakage determines the optimal working point for X -rotations.

To gain some analytical insight into this effect, we next present the noise-averaged solution to the qubit equations of motion that captures the effects of fluctuating precession axes. Since the qubit Hamiltonian is analogous to that of a single spin in an effective noisy magnetic field, we apply the solution to the dissipative dynamics of a single electron spin in an external magnetic field due to inhomogeneous broadening given in Ref. [12]. As noted above, near the sweet spot ϵ_X , all relevant noise sources have variance $\sigma \sim \text{neV}$, so that $\sigma/\Delta B_x \sim 1\%$. Therefore, we present this solution to the leading order in $\sigma/\Delta B_x$.

Consider X -rotations with an initial state $|S\rangle=|\hat{\mathbf{z}}\rangle$, where we denote by $|\pm\hat{\mathbf{n}}\rangle$ a state up (+) or down (-) along the unit vector $\hat{\mathbf{n}}$ on the S - T_- Bloch sphere. Applying the results of Ref. [12] to X -rotations, we find the noise-averaged solution for pseudospin expectation value $\overline{\mathbf{s}}=\langle\boldsymbol{\tau}\rangle/2$,

$$\overline{\mathbf{s}}(t) = \frac{e^{-(t/T_2^{(X)*})^2}}{2} [(\cos(\omega_X t) + 2\delta_{\perp}^2 \sin^2(\omega_X t/2)) \hat{\mathbf{z}} - \sin(\omega_X t) \hat{\mathbf{y}}], \quad (\text{D12})$$

where $\omega_X = b/\hbar$, $b = g\mu_B |\Delta B_x|/\sqrt{2}$,

$$\frac{\sqrt{2}\hbar}{T_2^{(X)*}} = \sigma_h, \quad \delta_{\perp}^2(\Delta B_x, B_z) = \frac{\sigma_J^2 + \sigma_h^2}{b^2}, \quad (\text{D13})$$

and σ_J is given in Eq. (D8). The probability of being in $|T_-\rangle$ is given by $P'_- = 1/2 - \overline{s_z}$. At the end of the π rotation period $\tau_X = \pi/\omega_X$, we find

$$P'_-(\tau_X) = \frac{1 + e^{-(\tau_X/T_2^*)^2} [1 - \delta_{\perp}^2(\Delta B_x, B_z)]}{2}, \quad (\text{D14})$$

where the prime on P'_- indicates that this quantity was calculated with the approximate formula Eq. (D12), to be distinguished from P_- computed by numerical simulations described in Sec. C. Thus, the main effect of the transverse noise fields is to reduce the P'_- amplitude by an amount of order δ_{\perp}^2 , which is maximum at the end of the π pulse (See Eq. (D12)). The infidelity $1 - P'_-$ as a function of B_z is plotted in the inset (right axes) of Fig. 2(a) in the main text, and is consistent with our numerical simulations of $1 - P_-$, shown in the main panel of Fig. 2(a) in the main text.

Appendix E: Dephasing in the far-detuned regime

In this section, we present an analytic solution for Z' rotations, which can be used to extract the purely nuclear noise-dominated dephasing time from experimental data. The results are valid for arbitrary values of the applied magnetic fields.

In the physically relevant 4×4 subspace described in Sec. A, the Hamiltonian can be written in the Heisenberg form

$$H = J(\epsilon) \left(\mathbf{S}_L \cdot \mathbf{S}_R - \frac{1}{4} \right) + g\mu_B \sum_{i=L,R} (\mathbf{B}_i + \mathbf{h}_i) \cdot \mathbf{S}_i. \quad (\text{E1})$$

In the far-detuned limit ($\epsilon \rightarrow -\infty$), only (1,1) charge states are occupied, and the exchange coupling J can be neglected. In this case, the system dynamics corresponds to individual spins precessing about their local magnetic fields, for which the time evolution operator is given by

$$\begin{aligned} U(t) &= \exp(i\omega_L t \hat{\mathbf{n}}_L \cdot \boldsymbol{\sigma}_L) \otimes \exp(i\omega_R t \hat{\mathbf{n}}_R \cdot \boldsymbol{\sigma}_L) \\ &= \cos \omega_L t \cos \omega_R t + i \cos \omega_L t \sin \omega_R t \sum_{i=L,R} \hat{\mathbf{n}}_i \cdot \boldsymbol{\sigma}_i - \sin \omega_L t \sin \omega_R t (\hat{\mathbf{n}}_L \cdot \boldsymbol{\sigma}_L) \otimes (\hat{\mathbf{n}}_R \cdot \boldsymbol{\sigma}_R), \end{aligned}$$

where

$$\boldsymbol{\omega}_i = \frac{g\mu_B |\mathbf{B}_i + \mathbf{h}_i|}{2\hbar} \quad \text{and} \quad \hat{\mathbf{n}}_i = \frac{\mathbf{B}_i + \mathbf{h}_i}{|\mathbf{B}_i + \mathbf{h}_i|}, \quad (i = L, R),$$

and $\boldsymbol{\sigma}_L$ and $\boldsymbol{\sigma}_R$ denote the spin operators on the left and right dots, respectively. Note that these operators differ from the $\boldsymbol{\tau}$ operators previously defined for the logical qubits states.

Applying this solution to an initial state $|\hat{\mathbf{x}}\rangle$, we calculate the probability $P_{-x}(t) = \overline{|\langle -\hat{\mathbf{x}} | U(t) | \hat{\mathbf{x}} \rangle|^2}$ of occupying $|-\hat{\mathbf{x}}\rangle$ after a Z' -rotation, where the average is taken over all nuclear fields $\mathbf{h}_{L,R}$. The relevant amplitudes are readily

computed:

$$\begin{aligned}
\langle -\hat{\mathbf{x}}|U(t)|\hat{\mathbf{x}}\rangle &= \frac{1}{2}(\langle S|U|S\rangle - \langle T_-|U|T_- \rangle + 2i \operatorname{Im}[\langle S|U|T_- \rangle]), \\
\langle S|U(t)|S\rangle &= \cos \omega_L t \cos \omega_R t + \sin \omega_L t \sin \omega_R t (\hat{\mathbf{n}}_L \cdot \hat{\mathbf{n}}_R), \\
\langle S|U(t)|T_- \rangle &= \frac{1}{\sqrt{2}} [\sin \omega_L t \sin \omega_R t (n_L^z n_R^+ - n_L^+ n_R^z) - i \cos \omega_L t \sin \omega_R t (n_L^+ - n_R^+)], \\
\langle T_-|U(t)|T_- \rangle &= \cos \omega_L t \cos \omega_R t - i \cos \omega_L t \sin \omega_R t (n_R^z + n_L^z) - \sin \omega_L t \sin \omega_R t (n_L^z n_R^z),
\end{aligned} \tag{E2}$$

where $n_i^\pm = n_i^x \pm i n_i^y$ ($i = L, R$).

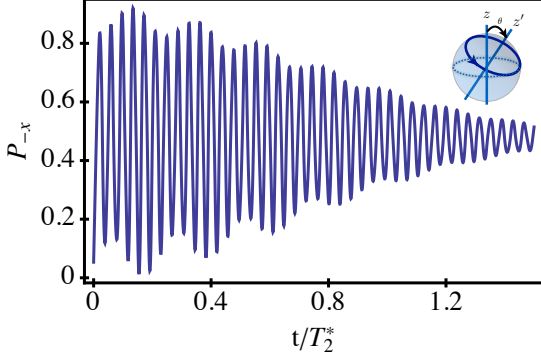


FIG. 7: The probability P_{-x} of being in state $|-\hat{\mathbf{x}}\rangle$ as a function of time t , for Z' -rotations around the equator of the Bloch sphere in the far-detuned regime where $J(\epsilon) \approx 0$. Solutions are obtained by numerically averaging the analytic solution given in Eq. (E2) over nuclear noise, for an initial state $|\hat{\mathbf{x}}\rangle$ and optimal magnetic fields $(\Delta B_x, B_z) = (0.25, 0.75) \mu\text{eV}$.

Note that the singlet probability in the second line of Eq. (E2) was previously calculated in Ref. [13]. The results of the P_{-x} calculation are plotted in Fig. S5 in time units of $T_2^* = \sqrt{2}\hbar/\sigma_h$. Here, we assume the optimal magnetic field values and $\Delta B_z = 0$, and we perform the nuclear average numerically.

The results shown in Fig. S5 are obtained for $J=0$. It is interesting to compare them with the analogous oscillations, for $J>0$, which are plotted in the inset of Fig. 2(c) in the main text. The most striking feature of the $J=0$ oscillations is the modulation of the oscillations, due to leakage. This modulation is the reason that the second sweet spot, corresponding to $\epsilon \rightarrow \infty$, is not an optimal working point for Z' -rotations, as noted in the main text. However, the visibility of the oscillations, defined as their maximum amplitude, is nearly unaffected. Here, the visibility is given by $|c_{-x}(\tau_{Z'})|^2 = \cos^2 \theta = \hat{\mathbf{z}} \cdot \hat{\mathbf{z}}'$, where θ is the angle between the axis of rotation ($\hat{\mathbf{z}}'$) and the z -axis ($\hat{\mathbf{z}}$) on the $S-T_-$ Bloch sphere, and $\tau_{Z'} = \pi\hbar/g\mu_B \sqrt{B_z^2 + B_x^2}/2$ is the π rotation period.

¹ W. A. Coish and D. Loss, Phys. Rev. B **72**, 125337 (2005).
² H. Ribeiro and G. Burkard, Phys. Rev. Lett. **102**, 216802 (2009).
³ We assume the valley mixing energies are much larger than the tunnel coupling so that the excited valley states can be neglected.
⁴ B. M. Maune, M. G. Borselli, B. Huang, T. D. Ladd, P. W. Deelman, K. S. Holabird, A. A. Kiselev, I. Alvarado-Rodriguez, R. S. Ross, A. E. Schmitz, M. Sokolich, C. A. Watson, M. F. Gyure, and A. T. Hunter, Nature **481**, 344 (2012).
⁵ O. E. Dial, M. D. Shulman, S. P. Harvey, H. Bluhm, V. Umansky, and A. Yacoby, Phys. Rev. Lett. **110** (2013).
⁶ M. Prada, R. H. Blick, and R. Joynt, Phys. Rev. B **77**, 115438 (2008), C. Tahan and R. Joynt, Phys. Rev. B **71**, 075315 (2005), *ibid* Phys. Rev. B **89** 075302 (2014).
⁷ P. Löwdin, The Journal of Chemical Physics **19**, 1396 (1951).

⁸ L. V. C. Assali, H. M. Petrilli, R. B. Capaz, B. Koiller, X. Hu, and S. Das Sarma, Phys. Rev. B **83**, 165301 (2011).
⁹ D. Kim, Z. Shi, C. B. Simmons, D. R. Ward, J. R. Prance, T. S. Koh, J. K. Gamble, D. E. Savage, M. G. Lagally, M. Friesen, S. N. Coppersmith, and M. A. Eriksson, Nature **511**, 70 (2014).
¹⁰ J. Sakurai, *Modern Quantum Mechanics* (Addison-Wesley, 1994).
¹¹ S. D. Barrett and C. H. W. Barnes, Phys. Rev. B **66**, 125318 (2002).
¹² I. A. Merkulov, A. L. Efros, and M. Rosen, Phys. Rev. B **65**, 205309 (2002).
¹³ J. M. Taylor, J. R. Petta, A. C. Johnson, A. Yacoby, C. M. Marcus, and M. D. Lukin, Phys. Rev. B **76**, 035315 (2007).